Thermal Cyclic Stress Analysis of a Solid Rocket Motor

Birkan Tunç* and Şebnem Özüpek†
Boğaziçi University, Istanbul, Turkey
Evgeny Podnos‡
Mechanics Software Inc., Austin, Texas 78751
and
Uğur Arkun§
Roketsan A. Ş., Elmadağ, Turkey

DOI: 10.2514/1.A34237

A three-dimensional stress analysis of a rocket motor under cyclic temperature loading was performed. The novelty of the analysis lies in the use of a propellant constitutive model that accounts for the effects of viscoelasticity, large deformation, temperature, pressure, and softening in monotonic and cyclic loadings. The material model was validated for the cyclic effects in terms of stress as well as dilatation responses. The role of various damage model parameters in the cyclic response was investigated. The distributions of these parameters were found to be consistent with the stress–strain field predictions of the rocket motor analysis, indicating efficiency and stability of the computational algorithm. It was concluded that the formulation and its implementation enables realistic stress analysis of solid rocket motors under general loading and environmental conditions, providing valuable information for their life assessment.

Nomenclature

a_T	=	time–temperature shift function
$\boldsymbol{C}$	=	right Cauchy–Green strain tensor
c, $c_{\max}$	=	void content and its maximum value
c_1, c_2	=	shift function parameters
c_{10}	=	Neo–Hookean energy density coefficient
$\bar{\boldsymbol{E}}$	=	Green strain distortional part
$f(s_f)$	=	cyclic loading function
G, K	=	shear and bulk relaxation functions
G_0, K_0	=	initial shear and bulk moduli
G_∞, K_∞	=	equilibrium shear and bulk moduli
G_i, K_i	=	Prony coefficients of shear and bulk moduli
$g(s_g)$	=	damage function
$\bar{I}_{\gamma(t)}$, $\bar{I}_{\gamma\max}$	=	distortional deformation and its maximum value
$\bar{I}_1$, $\bar{I}_2$	=	invariants of deviatoric right Cauchy–Green strain tensor
$I_{1,\sigma}$, $I_{2,\sigma}$	=	invariants of Cauchy stress
J	=	volume change ratio
J_c	=	volume change ratio due to inelastic deformations
J_e	=	volume change ratio due to elastic deformations
J_{th}	=	volume change ratio due to thermal effects
$\bar{P}$	=	volumetric part of viscoelastic and elastic stresses
$\boldsymbol{S}$	=	viscoelastic second Piola–Kirchhoff stress
s_g, s_f	=	internal state variables
T, T_0	=	temperature and its reference value
U^0	=	volumetric part of strain energy density function
α_{th}	=	thermal expansion coefficient
γ	=	internal state variable
$\boldsymbol{\Pi}$	=	deviatoric part of elastic stresses
σ_{shear}, σ_{crit}	=	octahedral shear stress and its critical value
τ_i	=	characteristic times
$\bar{\psi}^0$	=	deviatoric part of strain energy density function
ω_i	=	damage model parameters

Received 15 March 2018; revision received 28 May 2018; accepted for publication 5 June 2018; published online 14 August 2018.

*Mechanical Engineering Department, 34342 Bebek; currently Post-Doctoral Researcher, ICES, University of Texas at Austin, Austin, TX; tuncbirkan@gmail.com.

†Associate Professor, Mechanical Engineering Department, 34342 Bebek; ozupek@boun.edu.tr (Corresponding Author).

‡Senior Scientist, 4410 Avenue C; evgeny@mechanicssoft.com.

§Director, Propulsion Systems Design, Ankara; uarkun@roketsan.com.tr.

I. Introduction

A RELIABLE service life prediction (SLP) of a rocket motor depends on the accurate determination of the stress and strain fields under typical storage conditions. Yearly and daily temperature variations during storage are of particular interest because the response of solid propellant is highly temperature-dependent. An essential requirement for an accurate stress analysis under thermal loading is a constitutive model that realistically represents the highly nonlinear propellant behavior. A realistic constitutive model will be useful for SLP if it is implemented in a computational tool, such as a finite element method. To minimize convergence difficulties that may result from mathematical nonlinearities, a robust and numerically stable implementation algorithm is needed. To be of practical use in the industry, the amount of test data required for model calibration should be minimal. A model satisfying these criteria was previously formulated by the authors in [1] along with a systematic verification and validation procedure proposed in [2]. Literature regarding propellant constitutive models and their computational implementation was surveyed in these publications.

In this paper, recent literature on propellant constitutive modeling and rocket motor stress analysis is reviewed with an emphasis on temperature effect considerations.

The following models use a linear viscoelastic framework and allow material moduli to vary with temperature as well as with other state variables. Chyuan [3] included the propellant nonlinearity by varying the bulk modulus as a function of compressive stresses. The study showed that, for compressive thermal stress states, consideration of a nonlinear bulk modulus significantly affects the response compared to a linear analysis with constant bulk modulus. Hur et al.'s [4] constitutive model is based on the calculation of effective shear and bulk moduli of a propellant including the effect of voids, in addition to those of the binder and particles. The moduli of the binder were assumed to depend on temperature and strain rate. The model was calibrated using data at various rates and temperatures, and its use outside the calibration strain rate and temperature range was not recommended. In addition, low-temperature representation of the propellant behavior needed further study. Deng et al. [5] performed a three-dimensional structural analysis of solid rocket motor (SRM) grain subjected to thermal loading represented via cyclic Fourier series. The relaxation modulus was modified to account for aging effects.

It was concluded that thermoviscoelastic effects dominated the mechanical behavior during short term, whereas aging affected the behavior in the long term.

In the following works, a temperature-dependent damage parameter or function is introduced in a linear viscoelastic formulation. Jinsheng et al. [6] proposed a constitutive model where damage was assumed to evolve as a function of temperature. The validation was based on uniaxial test data with homogeneous deformation. Wang et al. [7] investigated the behavior of propellants at low temperature and high strain rate. It was determined that the dominating damage mechanism in propellant depends on temperature and changes from dewetting and matrix tearing at room temperature to particle brittle fracture at low temperature. Therefore, damage evolution was considered to depend on temperature. The model accurately predicted uniaxial homogeneous deformations. Extensive test data were used only to determine model parameters; hence, further validation for tests not included in calibration is needed. The three-dimensional constitutive model of Huiru et al. [8] assumes Poisson's ratio to depend on time and temperature. The model was implemented into a commercial finite element code; however, validation against test data was not provided. Three-dimensional thermal cyclic and ignition pressurization analyses showed that Von Mises stress predictions with viscoelastic Poisson's ratio are significantly higher than those with constant Poisson's ratio. Xu et al. [9] modeled the effect of temperature by modifying the calculation of the reduced time used in time–temperature superposition. That is, in addition to the standard shift factor, a variable called zero time was defined. The latter takes into account the relaxation of the propellant during the ramp loading to the strain level at which stress relaxation test is conducted. The results had greater precision than the standard procedure that uses time–temperature shift factor only.

Han et al. [10] proposed time–temperature–damage superposition to account for mechanical aging due to temperature cycling during storage. Time–temperature equivalence was obtained through the shift factor calibrated with relaxation test data at various temperatures. Time–damage equivalence was established using relaxation test data at various strain levels. The model was validated for uniaxial constant-strain-rate tests.

The following experimental studies investigated short- and long-term effect of temperature on the propellant response. Extensive testing of SRM grain under thermal loading was carried to study aging [11]. Sensors placed at the grain–case interface measured temperature and bond stress throughout the cycles. According to measurements, during repeated cycles between cold and hot temperatures, peak stress decreased with each cycle, with the highest reduction being in the first cooldown. Based on the shift factor obtained from time–temperature equivalence, corrected strain rates for cyclic loading were calculated [12], and uniaxial test conditions equivalent to calculated rates were defined. Comparable results were obtained for relative changes of peak stresses in successive cycles. Liu and Thompson [13] presented experimental results for a high-performance propellant at various strain rates and temperatures. Based on dilatation measurements, it was concluded that, for the initial linear portion of the deformation, the material was almost incompressible, whereas at higher strain, volume change increased due to the formation of voids following interface debonding. Test data were conclusive regarding the dependence of the shear modulus on the strain rate and temperature, whereas those of the bulk modulus were found to be quite complex, partly due to difficulties involved in accurate measurement of the bulk behavior.

A few studies considered the temperature effect within the finite deformation framework. Constitutive models proposed by Jung and Youn [14] and Yun et al. [15] are based on a viscoelastic dewetting criterion that assumes a temperature-dependent adhesion energy. Both models were implemented in finite element software. Simulations of either implementation agree reasonably well with test data for uniaxial and biaxial loading at various rates and temperatures. Simulations of nonhomogeneous deformations were not provided in either publication.

Based on the preceding survey, it was concluded that the propellant constitutive models available in the literature were not assessed in terms of their applicability to service life prediction. In particular, three-dimensional stress analysis with damaging nonlinear viscoelastic constitutive model was not carried out for a rocket motor subjected to cyclic thermal loading.

The first objective of this work is to validate the constitutive model and its implementation for cyclic loading of a three-dimensional geometry. The second and main objective is to conduct three-dimensional stress analysis of a rocket motor under thermal cyclic loading. The effect of various model parameters and functions on the response will be evaluated by comparing the predictions with a finite-strain viscoelastic model that does not account for damage and cyclic softening.

The remainder of the paper is organized as follows. The basic (i.e., nondamaging) three-dimensional viscoelastic formulation and the damage model are summarized in Sec. II. Validation of the constitutive model for cyclic loading is presented in Sec. III. In Sec. IV, the predictions of a rocket motor subjected to thermal cyclic loading are given. Conclusions and future work are presented in Sec. V.

II. Constitutive Model

The three-dimensional nonlinear viscoelastic constitutive model described in this section represents the effects of strain rate, temperature, superimposed pressure, and cyclic loading on the stress and dilatational response of the propellant. The model is characterized by uncoupled deviatoric and volumetric responses and is expressed in terms of the second Piola–Kirchhoff stress as

$$\boldsymbol{S}(t) = J\boldsymbol{C}^{-1}\int_0^t \frac{K(\xi_t - \xi_\tau)}{K_0}\frac{\partial \bar{P}}{\partial \tau}\,\mathrm{d}\tau + f(s_f)\int_0^t \frac{G(\xi_t - \xi_\tau)}{G_0}\frac{\partial \boldsymbol{\Pi}}{\partial \tau}\,\mathrm{d}\tau \tag{1}$$

$$\text{with } \bar{P} = \frac{\partial U^0}{\partial J} \quad \text{and } \boldsymbol{\Pi} = g(s_g)J^{-2/3}\mathrm{DEV}\left(\frac{\partial \bar{\psi}^0}{\partial \bar{\boldsymbol{E}}}\right)$$

where $\mathrm{DEV}(\cdot) = (\cdot) - (1/3)[\boldsymbol{C}\colon(\cdot)]\boldsymbol{C}^{-1}$, and K and G are bulk and shear relaxation functions and are normalized by initial values K_0 and G_0. The effect of damage on the stress response is represented with the function $g(s_g)$.

U^0 and $\bar{\psi}^0$ are the volumetric and distortional parts of the energy function and are selected as

$$U^0 = \frac{1}{2}K(J_e - 1)^2 \quad \text{and} \quad \bar{\psi}^0 = c_{10}(\bar{I}_1 - 3) \tag{2}$$

$$\text{with } J_e = \frac{J}{J_{\text{th}}J_c}, \quad J_{\text{th}} = [1 + \alpha_{\text{th}}(T - T_0)]^3, \quad J_c = 1 + c(t)$$

where J_e, J_c, and J_{th} are the volume ratios due to elastic, inelastic, and thermal effects, respectively; α_{th} is the coefficient of thermal expansion; and $c(t)$ represents the volume change due to damage. Although various energy forms are available in the literature, $\bar{\psi}^0$ represents the undamaged material response, and for the propellant considered in this work, it is well represented as Neo–Hookean expressed in terms of $\bar{I}_1$, the deviatoric invariant of the right Cauchy–Green deformation tensor $\boldsymbol{C}$, and a single material parameter c_{10}.

Because of limitation of available test data, the propellant in this work is assumed to have thermorheologically simple behavior. The change of shear and bulk moduli with temperature is taken into account by replacing the actual time t by the reduced time $\xi(t)$, as shown in Eq. (1). The actual and reduced times are related to each other through the shift function a_T as

$$\xi_t = \xi(t) = \int_0^t \frac{\mathrm{d}\eta}{a_T[T(\eta)]} \tag{3}$$

A. Damage Model

The main mechanism of damage is assumed to be the formation of microcracks at the highly stressed particle–binder interface or the binder itself. Motivated by the experimental data, the damage is

Table 1 Material parameters of the constitutive model

Prony terms	Williams–Landel–Ferry	Hyperelastic coefficients	Parameters
G_i	T_0	c_{10}	ω_1, ω_2
G_∞	c_1	K_0	ω_3, ω_4
τ_i	c_2	— —	ω_5, ω_6
— —	— —	— —	σ_{crit}

associated with volume increase in an otherwise nearly incompressible material. This inelastic volume change is represented by variable $c(t)$, and its evolution is formulated as

$$\dot{c}(t) = \omega_2 \bar{I}_\gamma^{\omega_3}(t) e^{P(t)/\omega_1} \tag{4}$$

where the octahedral shear strain $\bar{I}_\gamma = (1/6)\sqrt{2\bar{I}_1^2 - 6\bar{I}_2}$ accounts for the effect of distortional deformation; the exponential term represents the superimposed pressure effect; and ω_1, ω_2, and ω_3 are material parameters. The effect of damage on the volumetric response is captured by softening the initial bulk modulus according to

$$K = \frac{K_0}{1 + \omega_4 K_0 c(t)}[1 - c(t)] \tag{5}$$

where ω_4 is a material parameter.

B. Damage Initiation and Evolution

In solid propellants subjected to monotonic loading at a constant strain rate, the volume increase coincides with softening of stress. Therefore, it is assumed that damage starts when the octahedral shear stress reaches a critical value [15], that is

$$\sigma_{\text{shear}} = \frac{1}{3}\sqrt{2I_{1,\sigma}^2 - 6I_{2,\sigma}} > \sigma_{\text{crit}} \tag{6}$$

where $I_{1,\sigma}$ and $I_{2,\sigma}$ are Cauchy stress invariants, and σ_{crit} is assumed to be rate- and temperature-independent.

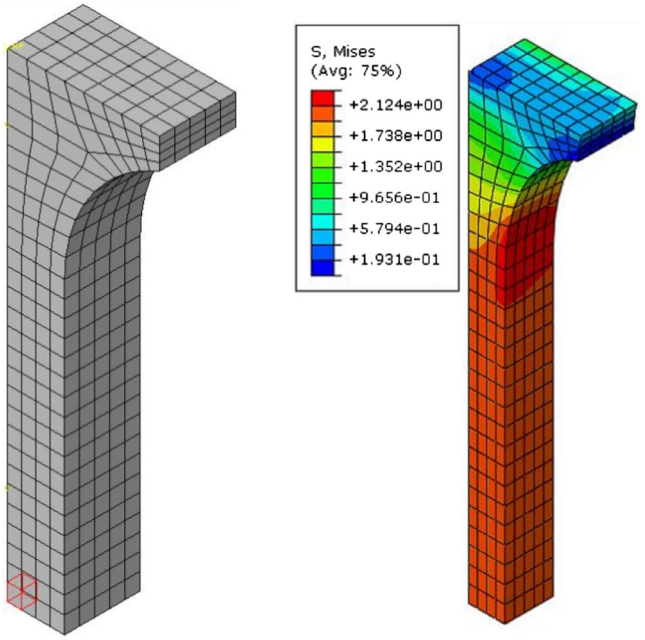

a) Finite element model of test specimen (field variables were evaluated for the marked element)

b) Von Mises stress (MPa) distribution

Fig. 1 Test specimen.

The amount of stress softening resulting from damage is represented with the function $g(s_g)$ introduced in Eq. (1). Because initiation of damage leads to volume increase and is assumed to be irreversible, the argument of the softening function is considered to be the maximum value of damage-related volume change reached

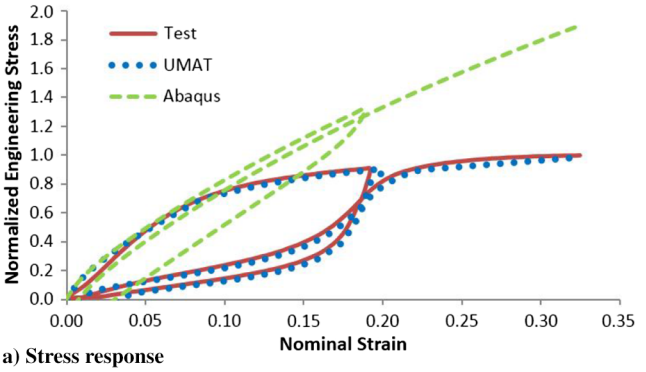

a) Stress response

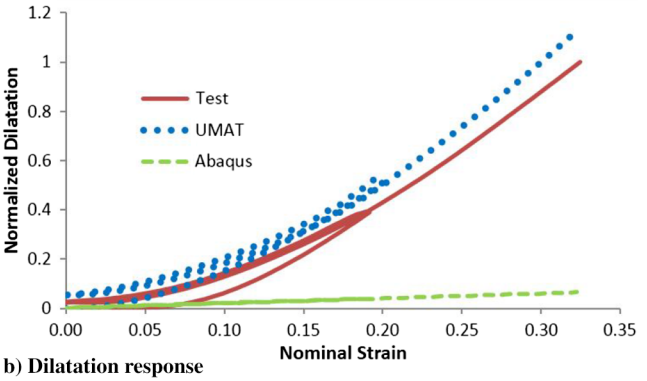

b) Dilatation response

Fig. 2 Uniaxial cyclic tensile test at 0.724 min^{-1} and 20°C with one cycle at 20% strain.

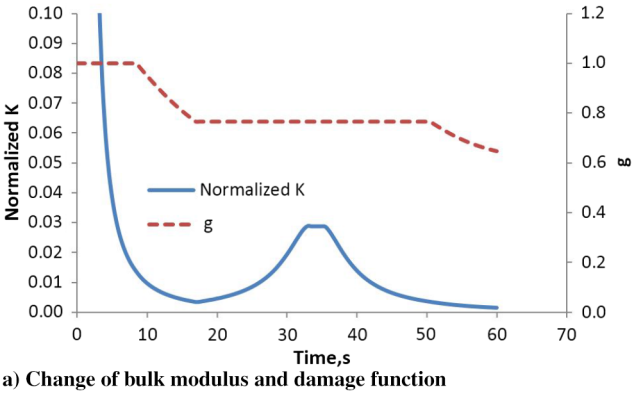

a) Change of bulk modulus and damage function

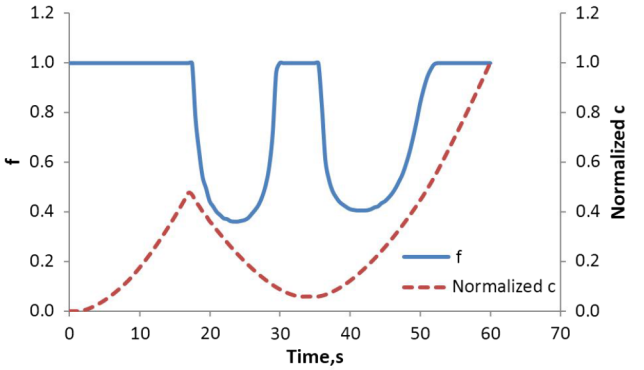

b) Change of cyclic softening function and void content

Fig. 3 Change of damage model parameters.

throughout the loading history. The rate of change of the function $g(s_g)$ with respect to s_g is proposed as

$$\frac{\mathrm{d}g(s_g)}{\mathrm{d}s_g} = \omega_5 \ell_n(s_g) e^{s_g/\omega_6} \tag{7}$$

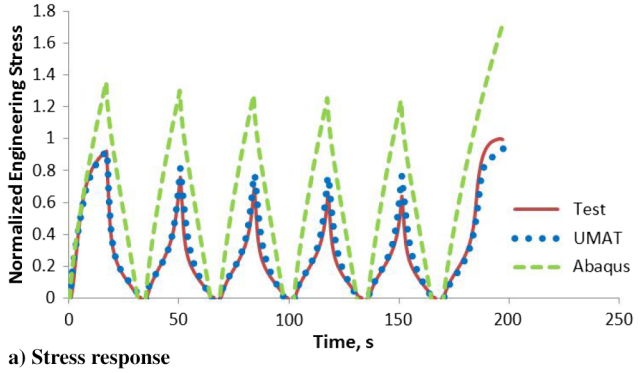

a) Stress response

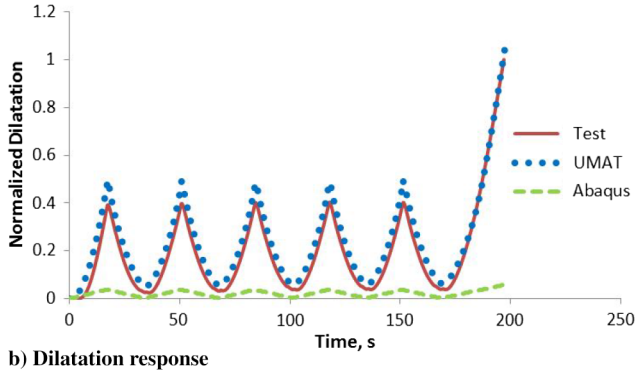

b) Dilatation response

Fig. 4 Uniaxial cyclic tensile test at 0.724 min^{-1} and 20°C with multiple cycles at 20% strain.

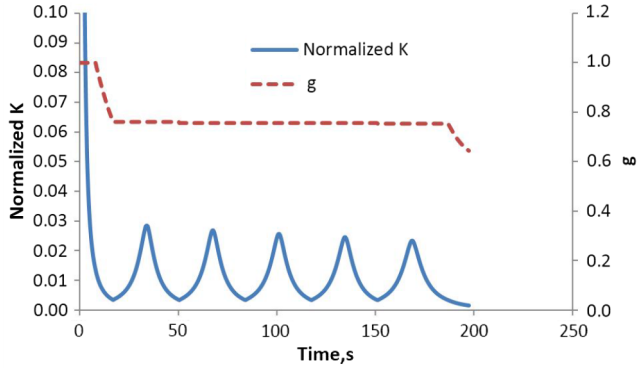

a) Change of bulk modulus and damage function

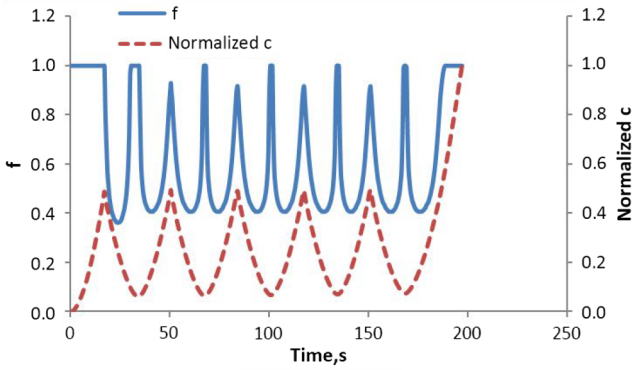

b) Change of cyclic softening function and void content

Fig. 5 Change of damage model parameters.

where ω_5 and ω_6 are material parameters. Although the parameters could be specific to each propellant batch, the shape of the function is general.

C. Cyclic Softening

Solid propellants subjected to cyclic uniaxial or biaxial loading at a constant strain rate show softening of stress during unloading and reloading. The cyclic hysteresis is greater than what viscoelasticity can account for. In the constitutive model described in this work, the cyclic softening is represented with the function $f(s_f)$, which modifies the viscoelastic deviatoric stress as shown in Eq. (1).

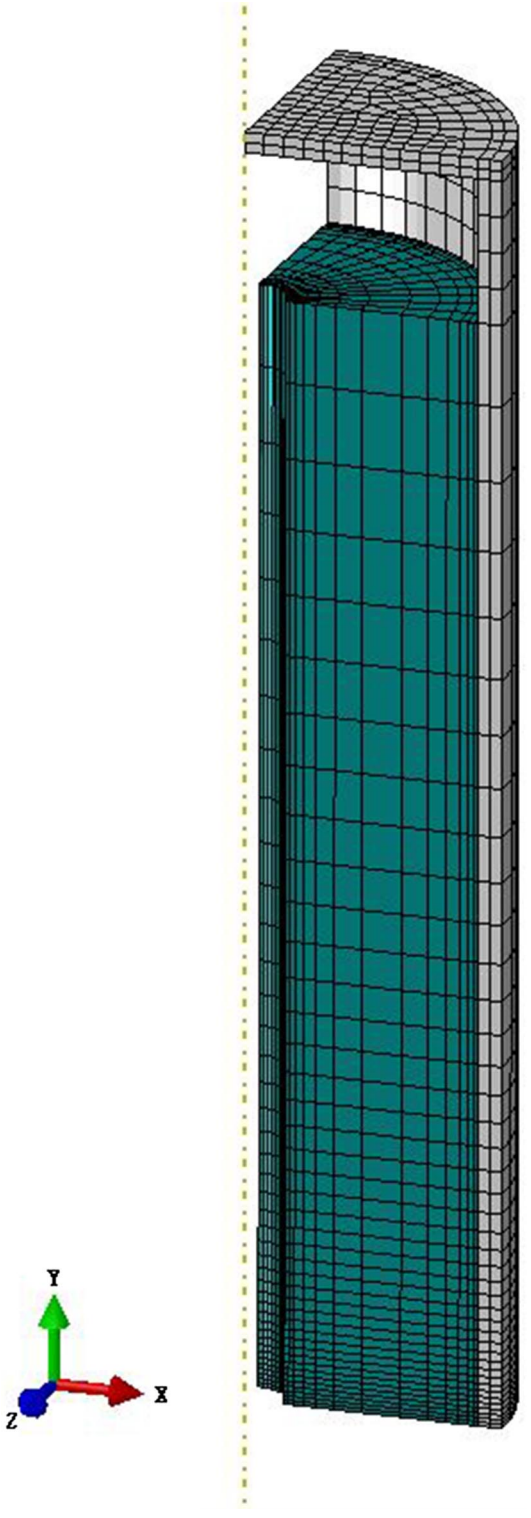

Fig. 6 Rocket motor model: steel casing and solid propellant grain.

The argument of $f(s_f)$ is defined as the ratio of the current octahedral shear strain to its maximum value within a cycle:

$$s_f = \frac{\bar{I}_\gamma}{\bar{I}_{\gamma_{\max}}} \tag{8}$$

The cyclic function proposed here has three distinct branches for loading, unloading, and reloading.

D. Calibration

The list of material parameters that were determined by fitting the constitutive model predictions to test data is shown in Table 1. The actual values are not given due to proprietary test data. A detailed calibration procedure can be found in [1].

III. Validation of Constitutive Model for Cyclic Loading

The constitutive model was implemented as a user-defined material (UMAT) into commercial finite element software [16].

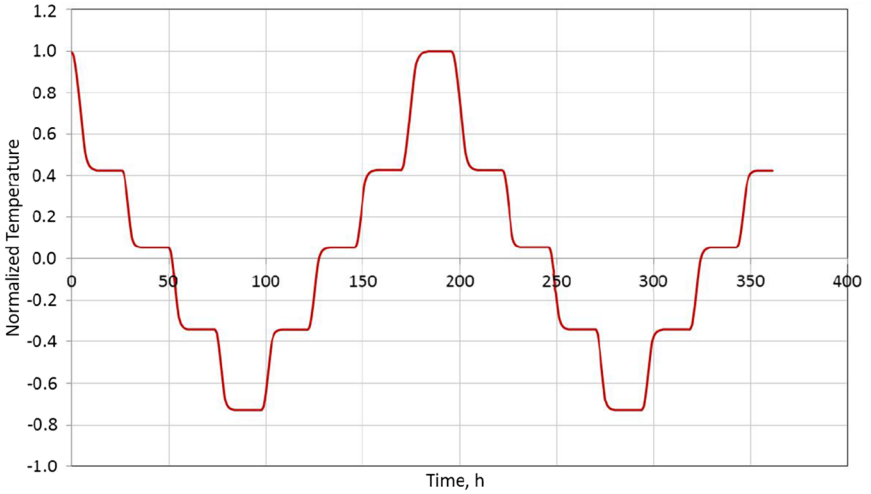

Fig. 7 Temperature history.

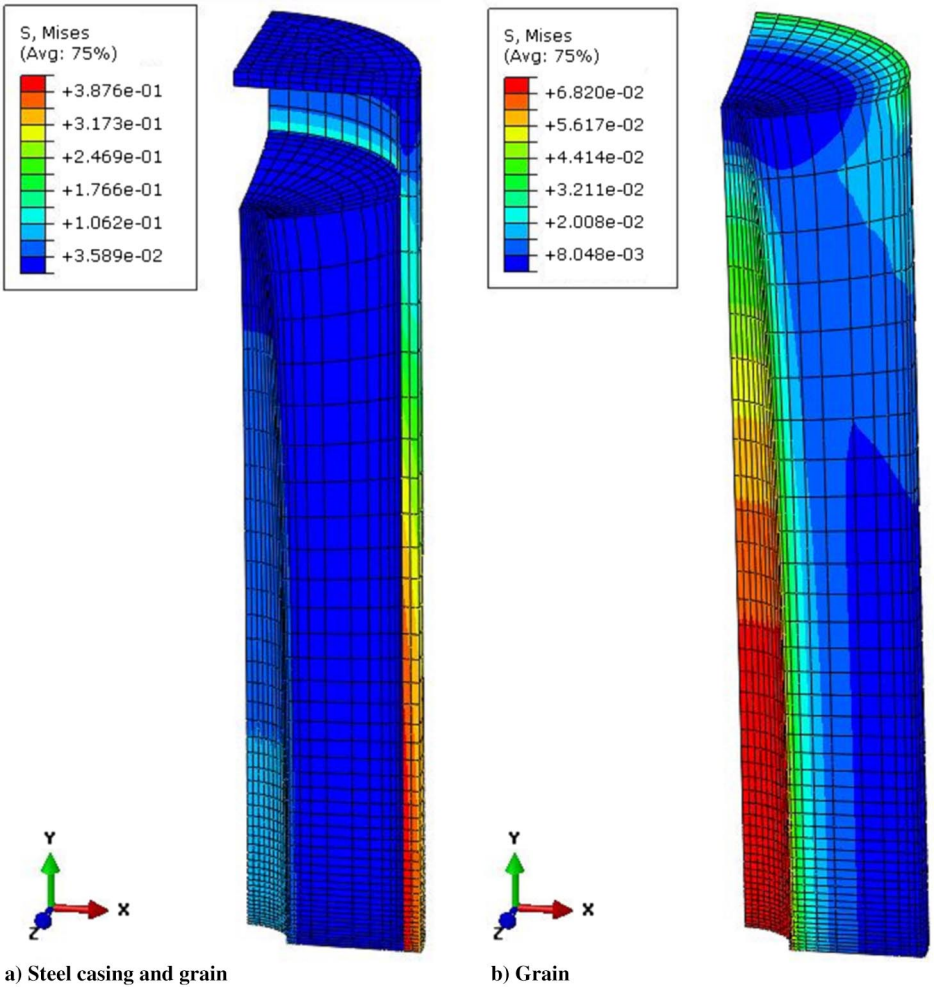

a) Steel casing and grain **b) Grain**

Fig. 8 Von Mises stress (in megapascals) distribution at the end of the analysis.

The implementation for the algorithm without damage was verified against the built-in material model available in the software. The damaging model was validated against test data. The verification and validation of the model, except for the cyclic softening, can be found in [2]. In the following, the predictive capability of the model for two cyclic loading scenarios is presented. In particular, loading to failure after a single cycle and loading to failure after multiple cycles were considered. To evaluate the robustness of the implementation,

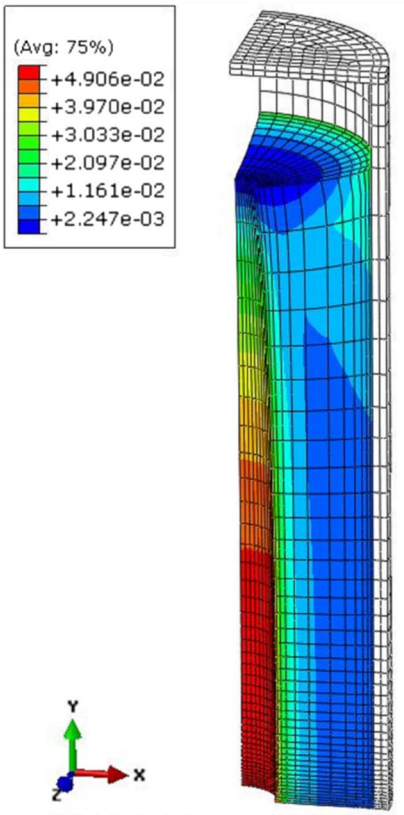

a) Octahedral shear strain $I_\gamma(t)$

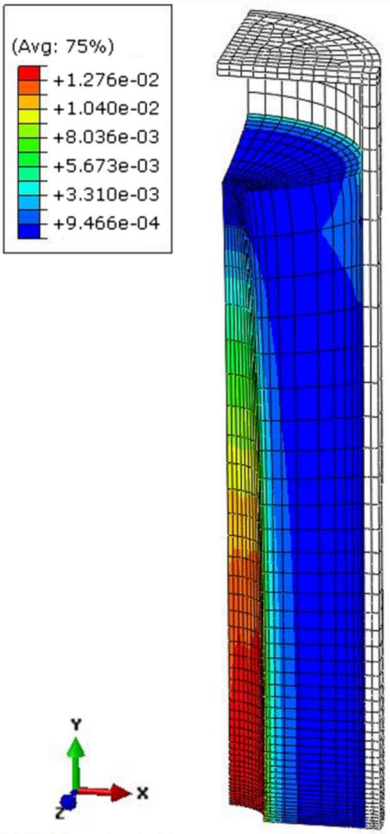

b) Void content $c(t)$

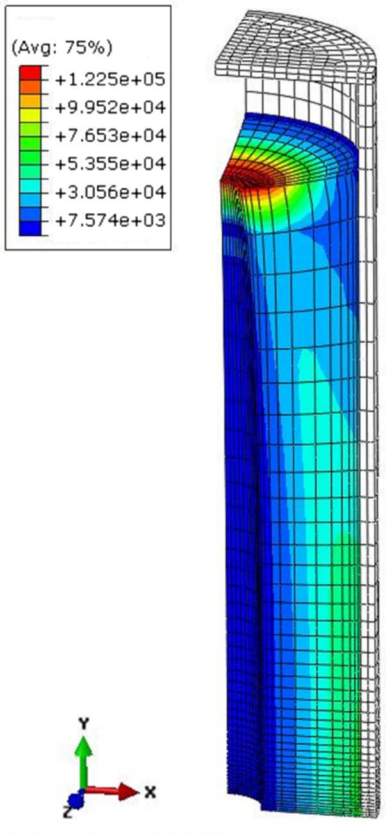

c) Bulk modulus $K(t)$ (MPa)

Fig. 9 Contour plots of state variables at the last time increment.

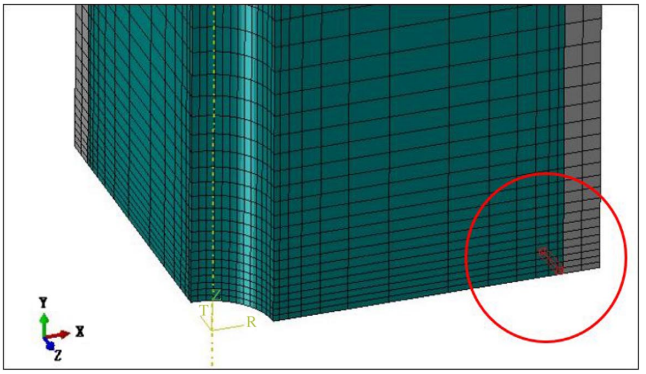

Fig. 10 Element where bond stress was evaluated.

a multi-element mesh was used. In particular, a finite element model of the test specimen was prepared and used in the study. The predictions of damaging model (UMAT) and nondamaging built-in model (ABAQUS) were compared to experimental data.

A. Cyclic Loading: Multi-Element, Single Cycle

One quarter of the test specimen was modeled by using linear fully integrated elements. Symmetry boundary conditions were applied at the x, y, and z planes. The loading consisted of a single cycle at 0.724 min^{-1} and 20°C. Figure 1 shows the finite element model of the specimen and the von Mises stress contour plot corresponding to the last increment. The values shown in the legend are for the nondamaging model. Stress and dilatation predictions at the location indicated in Fig. 1 are plotted in Fig. 2 against test data and nondamaging model predictions. All of the results were normalized with respect to the maximum value of data in the test results. The stress values compare quite well with the test data partially because the single cycle loading was used in the calibration of the unloading–reloading softening function. The agreement of the dilatational response is entirely due to good predictive capability of the model. Because the nondamaging model does not account for the stress softening due to dewetting and that driven by cyclic loading, its stress and dilatation predictions are not accurate. The history of void content and damage model parameters is shown in Fig. 3. Bulk modulus was normalized with respect to its initial value. Void content was normalized by its maximum during the loading history. It is noted that changes in both properties are not permanent, indicating that voids may open or close during loading.

B. Cyclic Loading: Multi-Element, Multiple Cycles

The test specimen model described in Sec. III.A was subjected to a uniaxial multiple cyclic loading. Predicted stress and dilatation histories are shown in Fig. 4. All results were normalized with respect to the maximum value of the corresponding test data. The stress and dilatation responses computed by the UMAT compare well with test data, whereas the nondamaging viscoelastic model overestimates the stress response and does not predict any dilatation. The history of various model parameters, normalized as described in Sec. III.A, is shown in Fig. 5. It can be observed that the bulk modulus value is greatly reduced during initial loading when damage is increasing due to newly forming voids. In subsequent cycles, when voids simply open or close, there is no further damage and hence no significant softening of the bulk modulus.

IV. Thermal Cyclic Analysis of Rocket Motor

In this section, finite element analysis of a rocket motor subjected to cyclic temperature loading is presented. In the following, first, the finite element model is detailed. Then, various results regarding predictions under thermal cyclic analysis are presented. Distribution of stress and constitutive model state variables is discussed.

A. Three-Dimensional Model of a Rocket Motor

The rocket motor analyzed consisted of the propellant grain and steel casing. Because of symmetry, only one eighth of the specimen was modeled as shown in Fig. 6. Three-dimensional quadratic reduced-integration brick elements were used to construct the finite element mesh. Symmetry boundary conditions were applied at the symmetry planes x, y, and z.

Temperature history shown in Fig. 7, normalized by the maximum value of temperature in the history, was uniformly applied to the motor assembly.

B. Results

The distribution of von Mises stress corresponding to the end of the thermal cycle is shown in Fig. 8 for the motor assembly and the grain. Maximum von Mises stress is obtained at the bore at the y symmetry plane. Figure 9 show contour plots of the octahedral strain $I_\gamma(t)$,

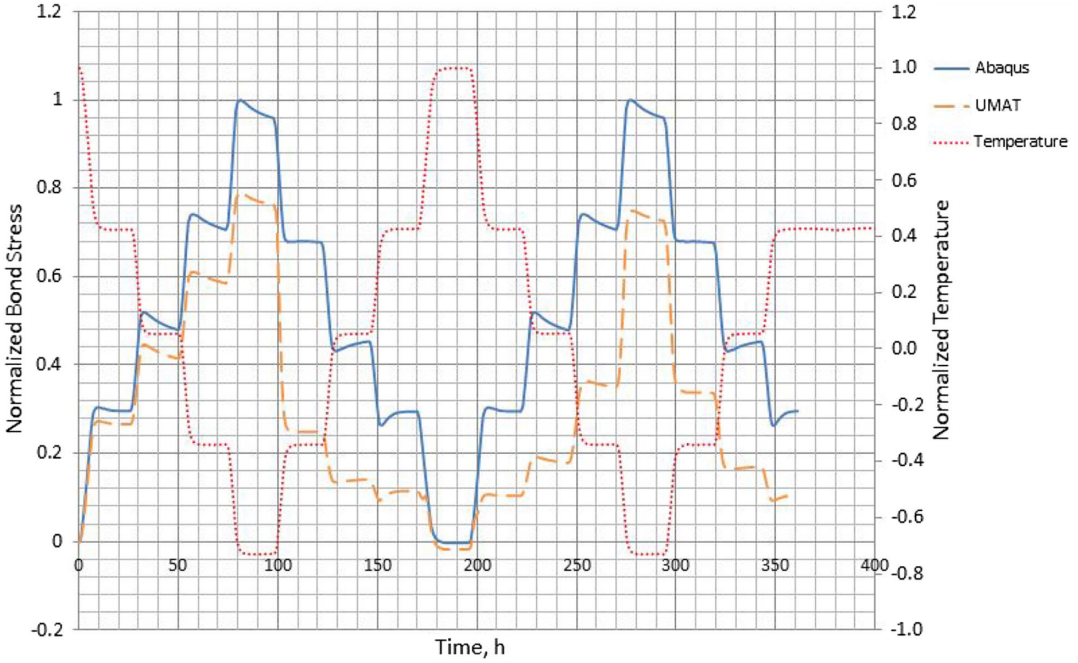

Fig. 11 Bond stress and temperature history.

void content $c(t)$, and bulk modulus $K(t)$. It is observed that all variables have a smooth variation. The distribution of the octahedral strain is similar to that of von Mises stress, and its maximum value occurs also at the bore at the y symmetry plane. Because $c(t)$ is proportional to $I_\gamma(t)$, the void content distribution is similar to that of the octahedral strain field. On the other hand, because bulk modulus decreases with the increase of void content, the minimum value of bulk modulus occurs at the location of maximum void content. Based on the consistency of the results, it is concluded that the material model and the computational algorithm are stable in performing three-dimensional thermal cyclic analysis of a rocket motor.

As stated in the literature review, dual stress and temperature (DBST) sensors [17] are being evaluated in the industry for health monitoring of SRMs. Typically, these sensors are installed at the grain–case interface and measure the bond stress and temperature throughout the life of the motor. Figure 10 shows an element at this interface where a DBST sensor would typically be installed. The bond stress history predicted at this location is shown in Fig. 11. ABAQUS predictions are also included for a more complete evaluation of the analysis. All stress values in the remainder of this section were normalized by the maximum value reached in the loading history with ABAQUS model. It is observed that the UMAT peak stress reached in each load cycle decreases from the first cycle to the next in accordance with DBST sensor data reported in the literature [18]. This capability of the model is due to the representation of the softening effects during unloading and reloading. The histories of the cyclic softening function $f(s_f)$ and its argument s_f are shown in Fig. 12. If this effect is not accounted for, the peak stress remains the same from cycle to cycle, as seen in ABAQUS results.

To further understand the difference in response between the built-in ABAQUS and the proposed model, the evolution of the damage

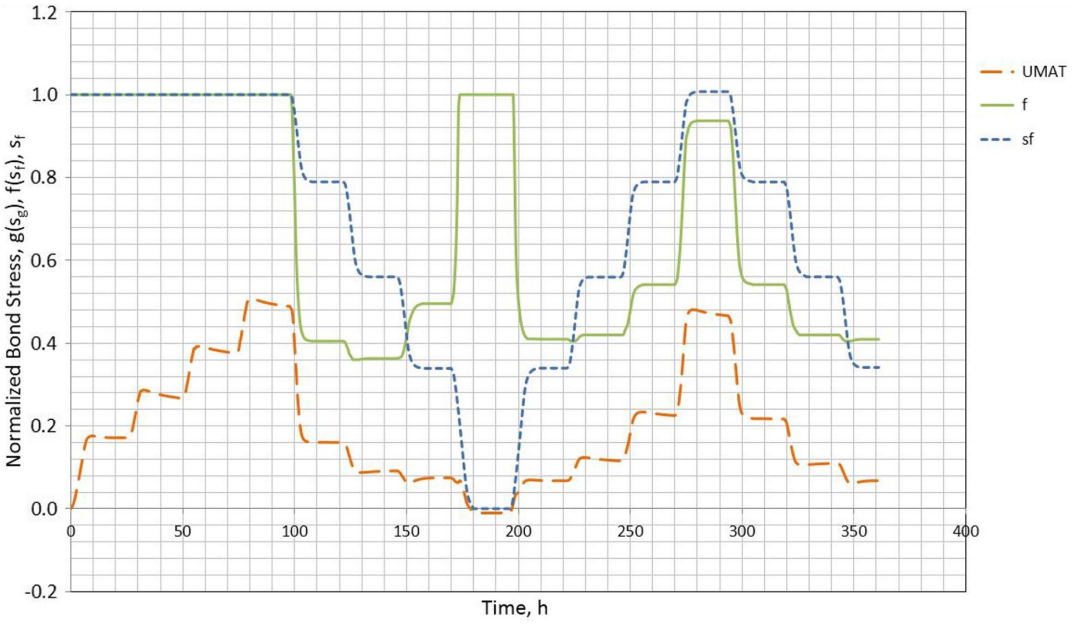

Fig. 12 Cyclic softening function history.

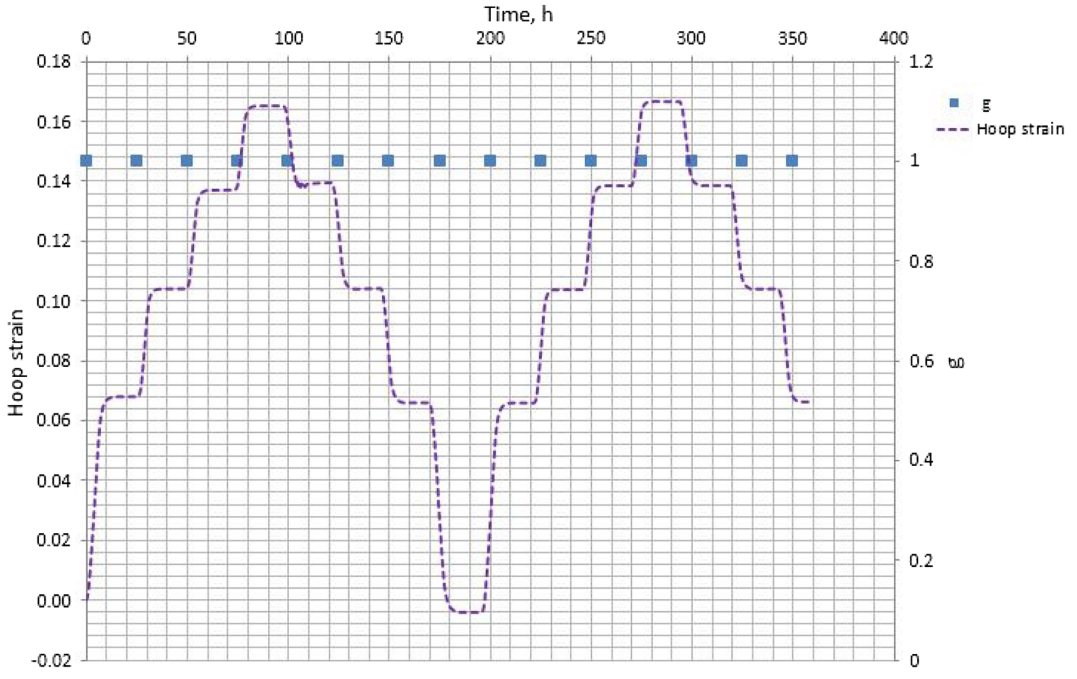

Fig. 13 Hoop strain history and softening function $g(s_g)$.

model parameters was investigated during the cooling part of the loading history. State variable $g(s_g)$ and hoop strain at the bore are shown in Fig. 13. It is observed that $g(s_g)$ remains equal to unity during the entire loading history even at the location of maximum hoop strain. Because this corresponds to the material response before the onset of damage, the difference between the two models is entirely due to modeling of the bulk behavior. This can be seen from the histories of state variable $c(t)$, the dilatation, and the bulk modulus, as shown in Fig. 14. It is observed that the void content increases, and as a consequence, bulk modulus decreases during the first cooling. It is therefore concluded that, even in the absence of $g(s_g)$, stress response softens due to the softening of the bulk modulus.

To quantify the effect of the softening bulk modulus on the stress response, an analysis with constant bulk modulus was carried out. The predictions are shown in Fig. 15. It is observed that the user material response is close to the built-in ABAQUS model for first cooling. Afterward, the responses differ due to the presence of cyclic softening function $f(s_f)$.

Another parameter worthy of investigation is the Neo–Hookean coefficient c_{10}. This parameter is determined from a single constant-strain-rate test. The data used in the calibration of the presented model were from a strain rate much higher than that in the thermal cycle loading used in this study. For transient thermal loading at slow rates, the stress is underpredicted [1]. Therefore, to evaluate the strain rate effect, Neo–Hookean coefficient c_{10} was recalibrated to data for uniaxial constant-strain-rate loading at 0.00724 min^{-1}, which was the slowest available test. The rest of the model parameters were kept the same. The bond stress predictions corresponding to calibration at two different rates are compared in Fig. 16. It is observed that the lower the temperature is, the greater the bondline stresses are.

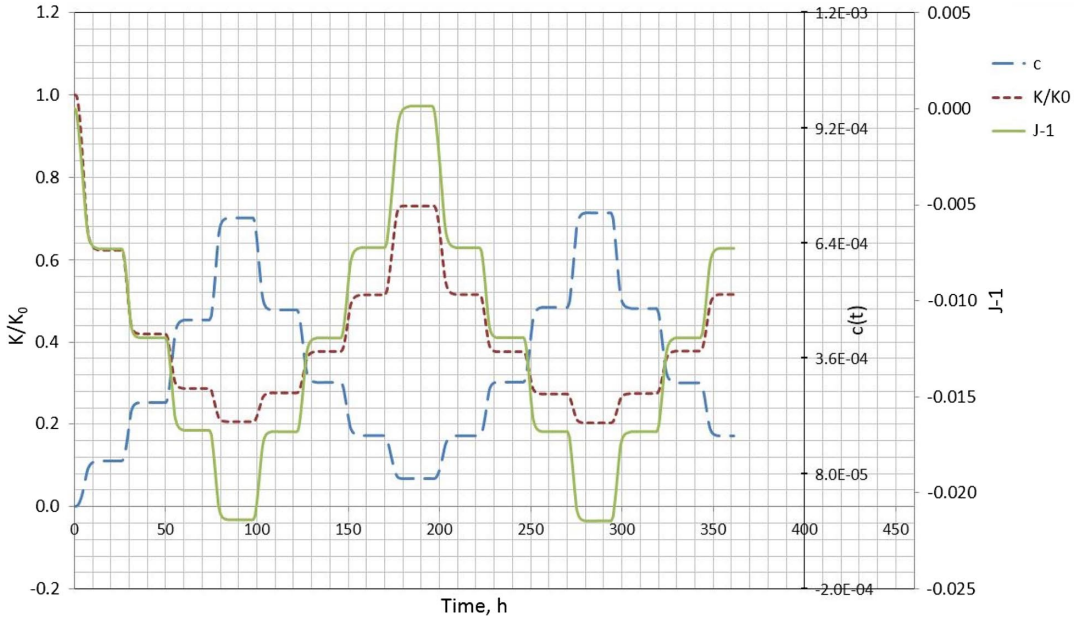

Fig. 14 Evolution of UMAT state variables.

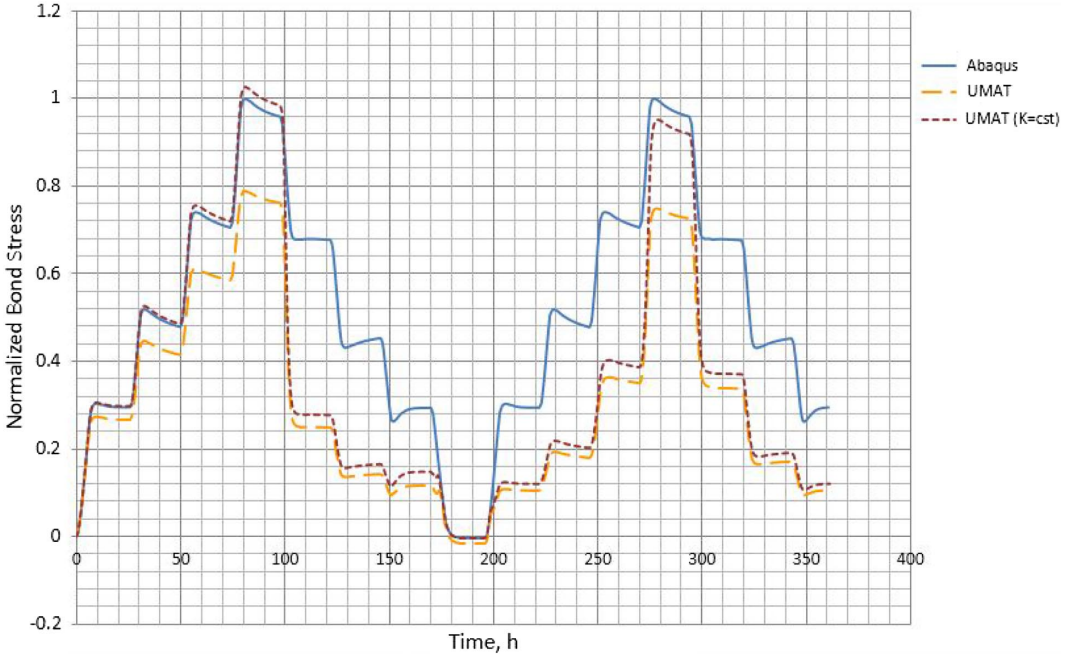

Fig. 15 Bond stress predictions for $K(t) = K_0$.

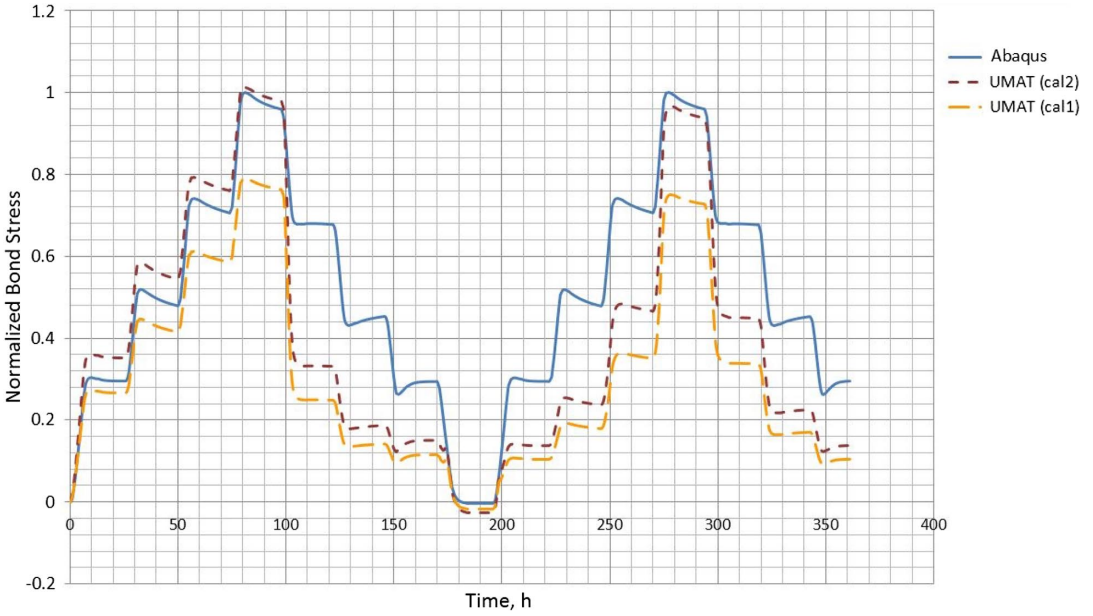

Fig. 16 Bond stress histories for a model calibrated at 0.724 min^{-1} (UMAT-cal1, ABAQUS) and 0.00724 min^{-1} (UMAT-cal2).

In summary, the proposed damaging model and the corresponding computational algorithm allowed to perform a three-dimensional finite element analysis of a rocket motor under cyclic temperature loading.

V. Conclusions

A three-dimensional nonlinear viscoelastic stress analysis of an analog solid rocket motor subjected to thermal loading was conducted. The constitutive model representing the propellant accounts for stress softening due to damage such as voids or microcracks as well as for softening during unloading–reloading. The modeling of the cyclic effect was validated using data from a uniaxial cyclic constant-strain-rate test. For the thermal cycle analysis, the peak stress reached in each load cycle decreased from first cycle to the next in accordance with test data from literature. It should be noted that the proposed model predicts the softening of the maximum stress only in the second cycle. After second cycle, no further decrease in the peak stress is predicted. Continuous decrease of stress in cyclic loading may be considered as leading to the end of service life, and it will be a topic of future research on reliability of solid rocket motor.

From a modeling point of view, comparison of the predictions with test data suggested that the damage mechanism for very slow rates may be different. This is important for simulation of storage conditions where the rate is very low compared to the typical range for test strain rates. Also, as future work, the predictions will be compared with measurements from sensor data. Reliability of sensor data and availability of both stress and strain measurements are important factors to be considered in such comparison. Thermorheologically complex material behavior or inclusion of rate-temperature effects in the damage model may be considered as part of model modifications to assure validity in a wider range of strain rates and temperatures.

Acknowledgments

The financial support of Boğaziçi University Research Fund (grant 11642) is gratefully acknowledged. The authors would like to express their appreciation to Roketsan A. Ş. for providing the test data.

References

[1] Tunç, B., and Özüpek, Ş., "Constitutive Modeling of Solid Propellants for Three Dimensional Nonlinear Finite Element Analysis," *Aerospace Science and Technology*, Vol. 69, Oct. 2017, pp. 290–297. doi:10.1016/j.ast.2017.06.025

[2] Tunç, B., and Özüpek, Ş., "Implementation and Validation of a Three Dimensional Damaging Finite Strain Viscoelastic Model," *International Journal of Solids and Structures*, Vols. 102–103, Dec. 2016, pp. 275–285. doi:10.1016/j.ijsolstr.2016.09.031

[3] Chyuan, S.-W., "Nonlinear Thermoviscoelastic Analysis of Solid Propellant Grains Subjected to Temperature Loading," *Finite Elements in Analysis and Design*, Vol. 38, No. 7, 2002, pp. 613–630. doi:10.1016/S0168-874X(01)00095-6

[4] Hur, J., Park, J.-B., Jung, G.-D., and Youn, S.-K., "Enhancements on a Micromechanical Constitutive Model of Solid Propellant," *International Journal of Solids and Structures*, Vol. 87, June 2016, pp. 110–119. doi:10.1016/j.ijsolstr.2016.02.025

[5] Deng, B., Xie, Y., and Tang, G. J., "Three-Dimensional Structural Analysis Approach for Aging Composite Solid Propellant Grains," *Propellants, Explosives, Pyrotechics*, Vol. 39, No. 1, 2014, pp. 117–124. doi:10.1002/prep.201300120

[6] Jinsheng, X., Xiong, C., Hongli, W., Jian, Z., and Changsheng, Z., "Thermo-Damage-Viscoelastic Constitutive Model of HTPB Composite Propellant," *International Journal of Solids and Structures*, Vol. 51, No. 18, 2014, pp. 3209–3217. doi:10.1016/j.ijsolstr.2014.05.024

[7] Wang, Z., Qiang, H., Wang, G., and Huang, Q., "Tensile Mechanical Properties and Constitutive Model for HTPB Propellant at Low Temperature and High Strain," *Journal of Applied Polymer Science*, Vol. 132, March 2015, pp. 1–9. doi:10.1002/app.42104

[8] Huiru, C., Guojin, T., and Zhibin, S., "A Three-Dimensional Viscoelastic Constitutive Model of Solid Propellant Considering Viscoelastic Poisson's Ration and Its Implementation," *European Journal of Mechanics A/Solids*, Vol. 61, Feb. 2017, pp. 235–244. doi:10.1016/j.euromechsol.2016.10.002

[9] Xu, J., Ju, Y., Han, B., and Zhou, C., "Research on Relaxation Modulus of Viscoelastic Materials Under Unsteady Temperature States Based on TTSP," *Mechanics of Time-Dependent Materials*, Vol. 17, No. 4, 2013, pp. 543–556. doi:10.1007/s11043-012-9203-z

[10] Han, L., Chen, X., Xu, J.-S., Zhou, C.-S., and Yu, J.-Q., "Research on the Time–Temperature–Damage Superposition Principle of NEPE Propellant," *Mechanics of Time-Dependent Materials*, Vol. 19, No. 4, 2015, pp. 581–599. doi:10.1007/s11043-015-9280-x

[11] Brouwer, G., Keizers, H., and Buswell, J., "Aging in Composite Propellant Grains," *40th AIAA/ASME/SAE/ASEE Joint Propulsion Conference and Exhibit*, AIAA Paper 2004-4058, July 2004. doi:10.2514/6.2004-4058

[12] Brouwer, G. R., Weterings, F. P., and Keizers, H., "Evaluation of Ageing in Composite Propellant Grains Part 2," *41st AIAA/ASME/SAE/ASEE*

Joint Propulsion Conference & Exhibit, AIAA Paper 2005-3803, July 2005.
doi:10.2514/6.2005-3803

[13] Liu, C., and Thompson, D., "Mechanical Response and Failure of High Performance Propellant (HPP) Subject to Uniaxial Tension," *Mechanics of Time-Dependent Materials*, Vol. 19, No. 2, 2015, pp. 95–115.
doi:10.1007/s11043-015-9254-z

[14] Jung, G.-D., and Youn, S.-K., "A Nonlinear Viscoelastic Constitutive Model of Solid Propellant," *International Journal of Solids and Structures*, Vol. 36, No. 25, 1999, pp. 3755–3777.
doi:10.1016/S0020-7683(98)00175-9

[15] Yun, K.-S., Park, J., Jung, G.-D., and Youn, S.-K., "Viscoelastic Constitutive Modeling of Solid Propellant with Damage," *International Journal of Solids and Structures*, Vol. 80, Feb. 2016, pp. 118–127.
doi:10.1016/j.ijsolstr.2015.10.028

[16] *ABAQUS User's Manual, Version 6.12*, Dassault Systems Simulia Corp., Providence, RI, 2012.

[17] Little, R., Chelner, H., and Buswell, H., "Development, Testing and Application of Embedded Sensors for Solid Rocket Motor Health Monitoring," *Proceedings of the 37th International Annual Conference of ICT*, Fraunhofer-Institut für Chemische Technologie, Karlsruhe, Germany, 2006.

[18] Brouwer, G. R., Buswell, H. J., and Chelner, H., "The Use of Embedded Bond Stress Sensors to Determine Aging," *43rd AIAA/ASME/SAE/ASEE Joint Propulsion Conference & Exhibit*, AIAA Paper 2007-5788, July 2007.
doi:10.2514/6.2007-5788

A. D. Ketsdever
Associate Editor